Earth Surface Processes and Landforms
Earth Surf. Process. Landforms **32**, 1558–1573 (2007)
Published online 30 January 2007 in Wiley InterScience
(www.interscience.wiley.com) **DOI:** 10.1002/esp.1490

Measuring streambank erosion due to ground water seepage: correlation to bank pore water pressure, precipitation and stream stage

Garey A. Fox,[1]* Glenn V. Wilson,[2] Andrew Simon,[2] Eddy J. Langendoen,[2] Onur Akay[1] and John W. Fuchs[1]

[1] *Department of Biosystems and Agricultural Engineering, Oklahoma State University Stillwater, OK, USA*
[2] *USDA-ARS National Sedimentation Laboratory, Oxford, MS, USA*

**Correspondence to:*
Garey A. Fox, Department of Biosystems and Agricultural Engineering, Oklahoma State University, 120 Agricultural Hall, Stillwater, OK 74078-6016, USA.
E-mail: Garey.fox@okstate.edu

Abstract

Limited information exists on one of the mechanisms governing sediment input to streams: streambank erosion by ground water seepage. The objective of this research was to demonstrate the importance of streambank composition and stratigraphy in controlling seepage flow and to quantify correlation of seepage flow/erosion with precipitation, stream stage and soil pore water pressure. The streambank site was located in Northern Mississippi in the Goodwin Creek watershed. Soil samples from layers on the streambank face suggested less than an order of magnitude difference in vertical hydraulic conductivity (K_s) with depth, but differences between lateral K_s of a concretion layer and the vertical K_s of the underlying layers contributed to the propensity for lateral flow. Goodwin Creek seeps were not similar to other seeps reported in the literature, in that eroded sediment originated from layers underneath the primary seepage layer. Subsurface flow and sediment load, quantified using 50 cm wide collection pans, were dependent on the type of seep: intermittent low-flow (LF) seeps (flow rates typically less than 0·05 L min^{-1}), persistent high-flow (HF) seeps (average flow rate of 0·39 L min^{-1}) and buried seeps, which eroded unconsolidated bank material from previous bank failures. The timing of LF seeps correlated to river stage and precipitation. The HF seeps at Goodwin Creek began after rainfall events resulted in the adjacent streambank reaching near saturation (i.e. soil pore water pressures greater than −5 kPa). Seep discharge from HF seeps reached a maximum of 1·0 L min^{-1} and sediment concentrations commonly approached 100 g L^{-1}. Buried seeps were intermittent but exhibited the most significant erosion rates (738 g min^{-1}) and sediment concentrations (989 g L^{-1}). In cases where perched water table conditions exist and persistent HF seeps occur, seepage erosion and bank collapse of streambank sediment may be significant. Copyright © 2007 John Wiley & Sons, Ltd.

Keywords: bank stability; interflow; ground water seepage; soil pore water pressure; streambank erosion

Received 28 September 2006;
Revised 5 December 2006;
Accepted 12 December 2006

Introduction

Research has demonstrated that streambank erosion contributes significantly (i.e. 30–80%) to total sediment loading in streams (Evans *et al.*, 2006; Sekely *et al.*, 2002; Simon and Darby, 1999; Bull, 1997). Predictive relationships and models generally view streambank erosion as the result of fluvial entrainment during stream flow (a function of near-bank velocity gradient and shear stress distribution) and the resulting mass failure by gravity (Simon and Darby, 1999). Streambank erosion by stream flow is frequently modeled with an excess shear stress equation relating erosion rate (E_r) to the applied shear stress (τ) once a critical shear stress (τ_c) has been exceeded:

$$E_r = K_d(\tau - \tau_c)^a \quad (1)$$

where K_d is the erodibility coefficient and a is a power term, commonly assumed to be unity (Hanson and Simon, 2001; Hanson and Cook, 1997). Streambank stability equations attempt to determine failure or collapse dependent upon a factor of safety, which is calculated as the ratio of driving to resistive forces (Thorne and Abt, 1993; Osman and Thorne, 1988). Gravitational forces tend to decrease stability while the forces of friction and cohesion resist sediment movement. Recent conceptual models of streambank stability include the role of saturated and unsaturated soil pore water pressures. When streambanks are unsaturated, stability is enhanced (Simon *et al.*, 2000; Rinaldi and Casagli, 1999; Simon and Curini, 1998; Darby and Thorne, 1996). Work has also been aimed at quantifying the role of riparian vegetation on streambank stability (Langendoen *et al.*, 2005; Simon and Collison, 2002).

Soil pore water pressures have been measured in relation to streambank stability and mass failure (Rinaldi *et al.*, 2004; Simon *et al.*, 2000; Casagli *et al.*, 1999; Simon and Curini, 1998). Several studies report ground water sapping (Simon *et al.*, 1999; Hagerty, 1991a); however, only a few studies to date, for example Wilson *et al.* (2007), report *in situ* seepage flow and erosion measurements. Sapping or seepage erosion occurs when high infiltration rates cause the development of perched water tables above water-restricting horizons in riparian soils (Jones, 1997; Wilson *et al.*, 1991; Coates, 1990) or between layers with contrasting hydraulic conductivities (Hagerty, 1991a, 1991b). As perched water tables rise on these less permeable layers, large hydraulic gradients can initiate towards stream channels, causing fairly rapid subsurface flow (interflow) towards streams (Wilson *et al.*, 2007; Fox *et al.*, 2006; Wilson *et al.*, 1991). Seepage flow initiates development and headward migration of gullies by liquefaction of soil particles, followed by mass wasting of the stream bank by undercutting of the gully face (Wilson *et al.*, 2007; Fox *et al.*, 2006; Istanbulluoglu *et al.*, 2005; Lobkovsky *et al.*, 2004; Bryan *et al.*, 1998; Jones, 1997; Dunne, 1990; Howard and McLane, 1988; Iverson and Major, 1986; Higgins, 1984).

Fox *et al.* (2006) and Wilson *et al.* (2007) performed lysimeter experiments to simulate streambank undercutting by seepage flow and bank collapse. Flow rates and sediment concentrations from the lysimeter experiments were compared to seepage flow and erosion measurements at only one field site: Little Topashaw Creek in Northern Mississippi (Wilson *et al.*, 2007; Fox *et al.*, 2006; Periketi, 2005). Their research indicated that detailed characterization of soil profile lithology is critical for accurate seepage erosion prediction, but was limited in that the measurements were not correlated to precipitation, stream stage or streambank soil pore water pressure.

The objective of the research reported here was to demonstrate the importance of streambank composition and stratigraphy in controlling seepage flow and to quantify correlation between controlling hydrologic factors (precipitation, stream stage and soil pore water pressure) with seepage flow and erosion. The seeps measured at Goodwin Creek are unique from the seeps at Little Topashaw Creek and supplement the significantly limited database on streambank seepage erosion, even though seepage erosion is documented in numerous geographical locations. Also, unique from Little Topashaw Creek, these seep measurements could be directly correlated to precipitation, stream stage and streambank soil pore water pressure at various depths within the soil profile.

Materials and Methods

Site Description

Goodwin Creek drains a fourth-order, 21 km^2 northwest Mississippi watershed located along the bluffline of the Mississippi River Valley (Figure 1). The main channel of Goodwin Creek was channelized (straightened) prior to about 1940 and experienced severe incision between 1960 and 1980. At the monitoring site, channel width ranges from 20 to 70 m and depth ranges from 4 to 5 m. The parent material for soils in Goodwin Creek consists mainly of loess over coastal plain sediment. However, the soils in the stream bottoms are alluvial deposits, primarily of the loess parent material. Soil at the research site is characterized as Falaya silt loam, somewhat poorly drained, coarse-silty, mixed, active, acid, thermic Aeric Fluvaquents. Bank materials consist of about 2 m of moderately cohesive (cohesion, $c' = 2{\cdot}7$ kPa), structureless, brown (10YR 5/3), silt loam of late Holocene age overlying 1·5 m of blocky to prismatic loam of considerable cohesion ($c' = 6{\cdot}3$ kPa) and lower permeability of early Holocene age, with a thin (i.e. 0·1–0·2 m thick) layer consisting predominately of iron (Fe) and manganese (Mn) concretions (concretion layer) in between the late Holocene and early Holocene layers. These layers overlie 1 m of loamy sand and 1·5 m of packed sandy gravel. Soil and geotechnical parameters for the late Holocene and early Holocene layers have been reported by Langendoen *et al.* (2006) including cohesion, friction angle, bulk density, porosity and particle size distribution (Table I). Tensiometers (UMS, Munich, Germany) have been installed at Goodwin Creek to measure adjacent soil pore water pressure at 30 (T30), 100 (T100), 148 (T148), 200 (T200) and 270 (T270) cm below ground surface (bgs). Precipitation and stream stage are continuously monitored throughout the watershed (Figure 1).

DOI: 10.1002/esp

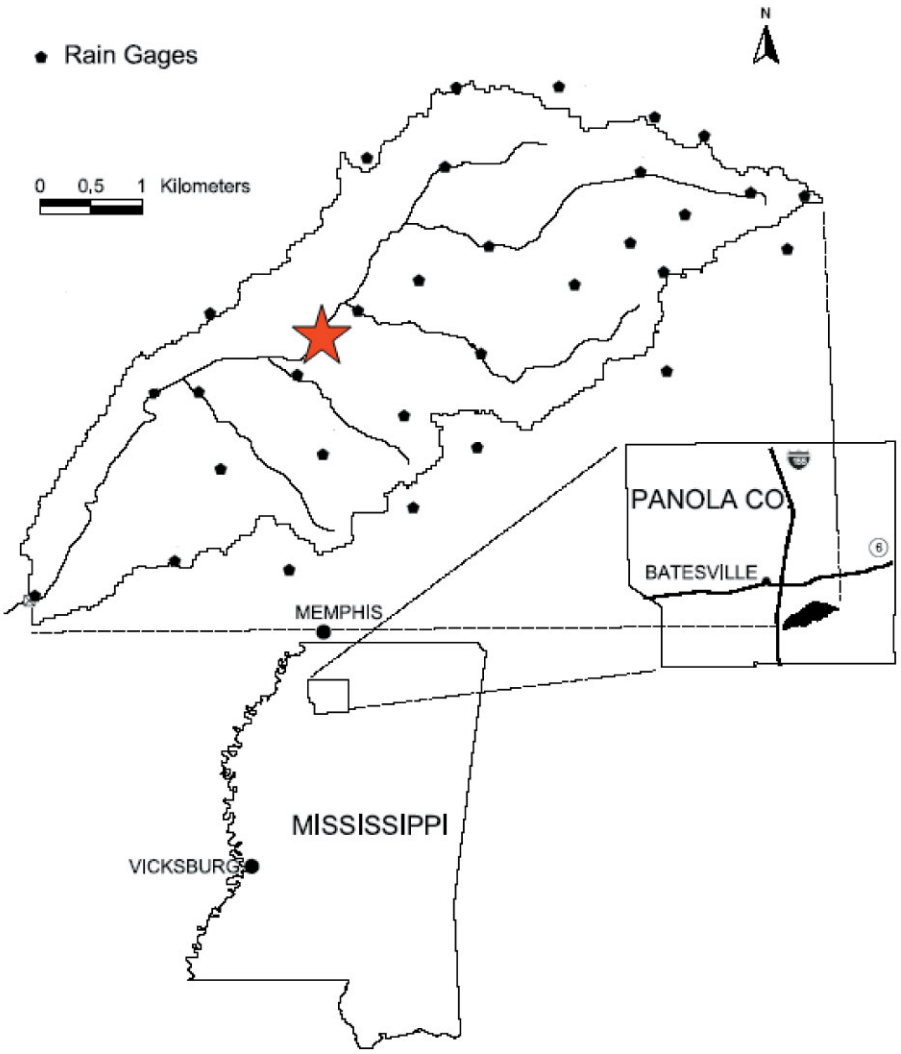

Figure 1. Map of Goodwin Creek experimental watershed. Modified from Bingner (1996). The star indicates the specific location of seepage erosion measurements. This figure is available in colour online at www.interscience.wiley.com/journal/espl

Table I. Streambank soil and geotechnical parameters at Goodwin Creek as reported by Langendoen *et al.* (2006)

	Soil layer	
Soil parameter	**Late Holocene (LH)**	**Early Holocene (EH)**
Thickness, m	1·7	1·5
USDA classification	Silt	Sandy loam/loam
Bulk density, ρ_b (g cm^{-3})	1·5	1·6
Cohesion, c' (kPa)	2·7	6·3
Friction angle, ϕ' (degrees)	28·1	27·0
% sand	5·1	52·1
% silt	91·1	41·8
% clay	3·8	6·1

DOI: 10.1002/esp

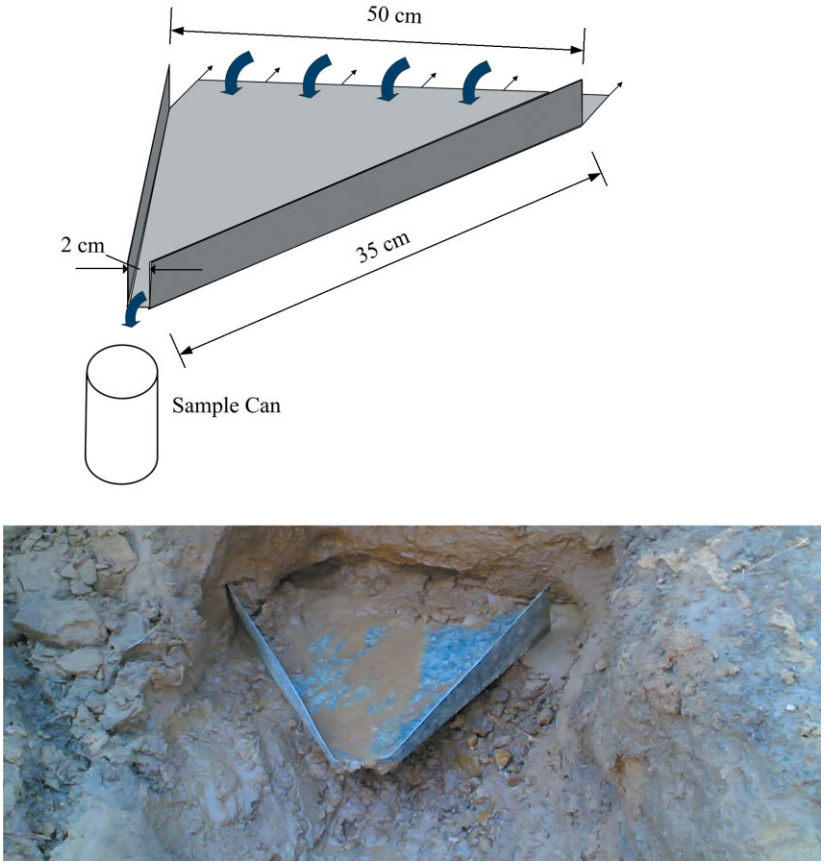

Figure 2. Lateral flow collection pan (i.e. mini-flume) utilized to measure streambank seepage flow and erosion. Flow and sediment are allowed to flow into the 50 cm wide pan until reaching steady state and then a discrete time interval sample of flow and sediment is collected at the 2 cm wide outflow face. This figure is available in colour online at www.interscience.wiley.com/journal/espl

Measuring Seepage Flow and Erosion

Subsurface flow and erosion was quantified at selected seep locations using lateral flow collection flumes (Figure 2) installed into exposed faces of the Goodwin Creek streambank, similar to the work of Wilson *et al.* (2007). Each flume had a 50 cm wide opening at the bank face with a lip inserted 10 cm into the bank. The sides were 10 cm high at the bank face and tapered down to 2 cm high at the 2 cm wide outflow end. Following rainfall events between 1 January 2006 and 1 May 2006, pans were installed at seep locations and water and sediment was allowed to flow though the collection pan until reaching steady state discharge. At steady state, a sample was collected in 0·5–1·0 L bottles, depending on the flow rate, over a discrete time interval. Most seeps were measured approximately 12–24 hr after the rainfall event to separate seepage flow from overland flow. Flow rates (L min^{-1}), erosion rates (g min^{-1}) and sediment concentrations (g L^{-1}) were determined with compensation for the sediment displacement volume. Seep locations studied at Goodwin Creek (Figure 3) included LF seeps (classified as those seeps with average flow rates less than 0·1 L min^{-1}) primarily active following large precipitation events and increases in stream stage (Figure 4), HF seeps (classified as those seeps with average flow rates greater than 0·1 L min^{-1}) active once the streambank reached near-saturation pore water pressure and continued until extended dry periods (Figure 4) and buried seeps located at HF seeps but emerging from previously sloughed bank material and active infrequently throughout the study period (Figure 5).

Streambank Sampling and Characterization

Vertically and horizontally oriented undisturbed soil cores were extracted along with disturbed soil samples from the late Holocene, concretion layer and the underlying early Holocene or loamy sand layers at two seep locations. The

DOI: 10.1002/esp

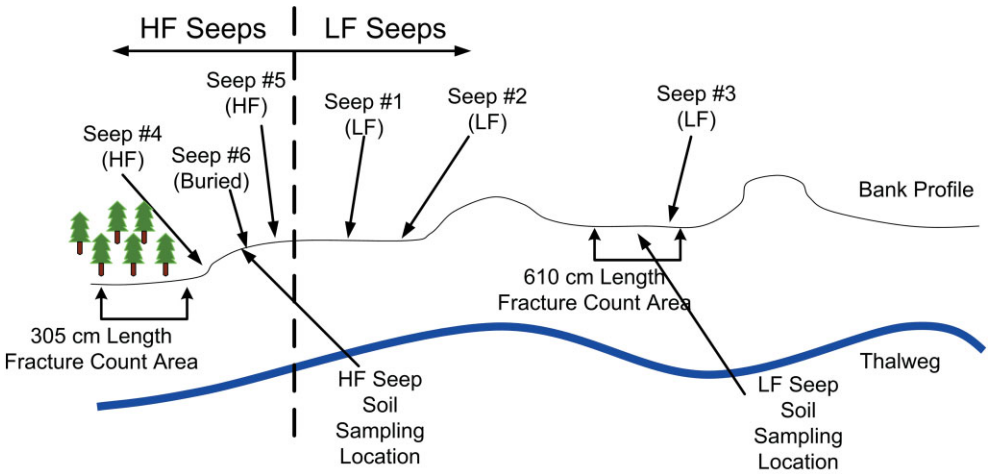

Figure 3. Sampling and seep locations at the Goodwin Creek experimental watershed. This figure is available in colour online at www.interscience.wiley.com/journal/espl

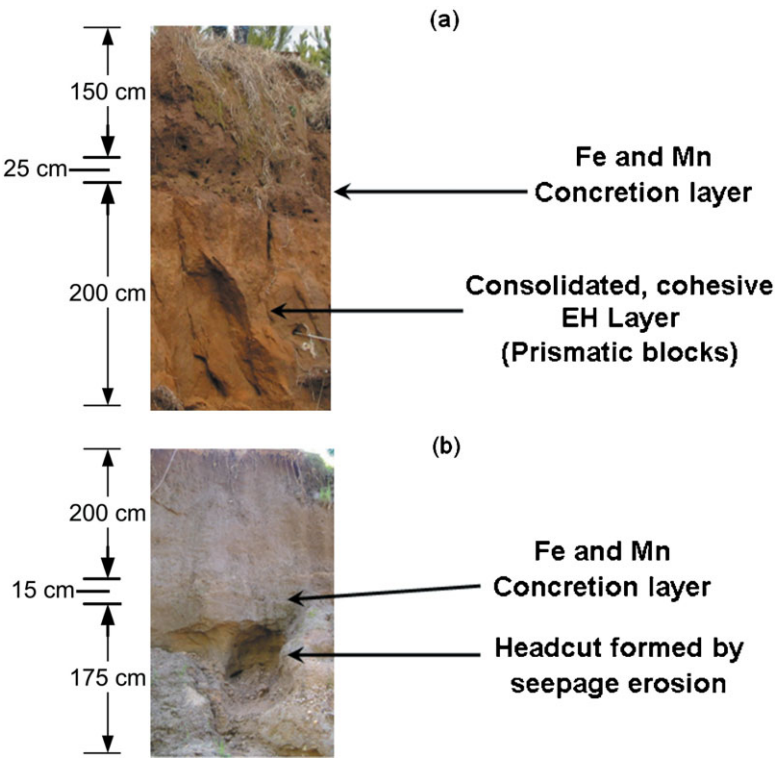

Figure 4. Streambank composition and stratigraphy at the (a) low-flow seeps and (b) high-flow seeps at Goodwin Creek. This figure is available in colour online at www.interscience.wiley.com/journal/espl

first location, Figure 3, corresponded to the location of LF seeps. Four replicate samples were obtained at each of the following depths: vertical samples at 25 cm bgs (late Holocene), vertical and horizontal samples at 95–100 cm bgs (late Holocene), vertical and horizontal samples at 150–175 cm bgs (Fe and Mn conductive concretion layer) and vertical samples at 190–200 cm bgs (early Holocene). The second location corresponded to the location of HF and

DOI: 10.1002/esp

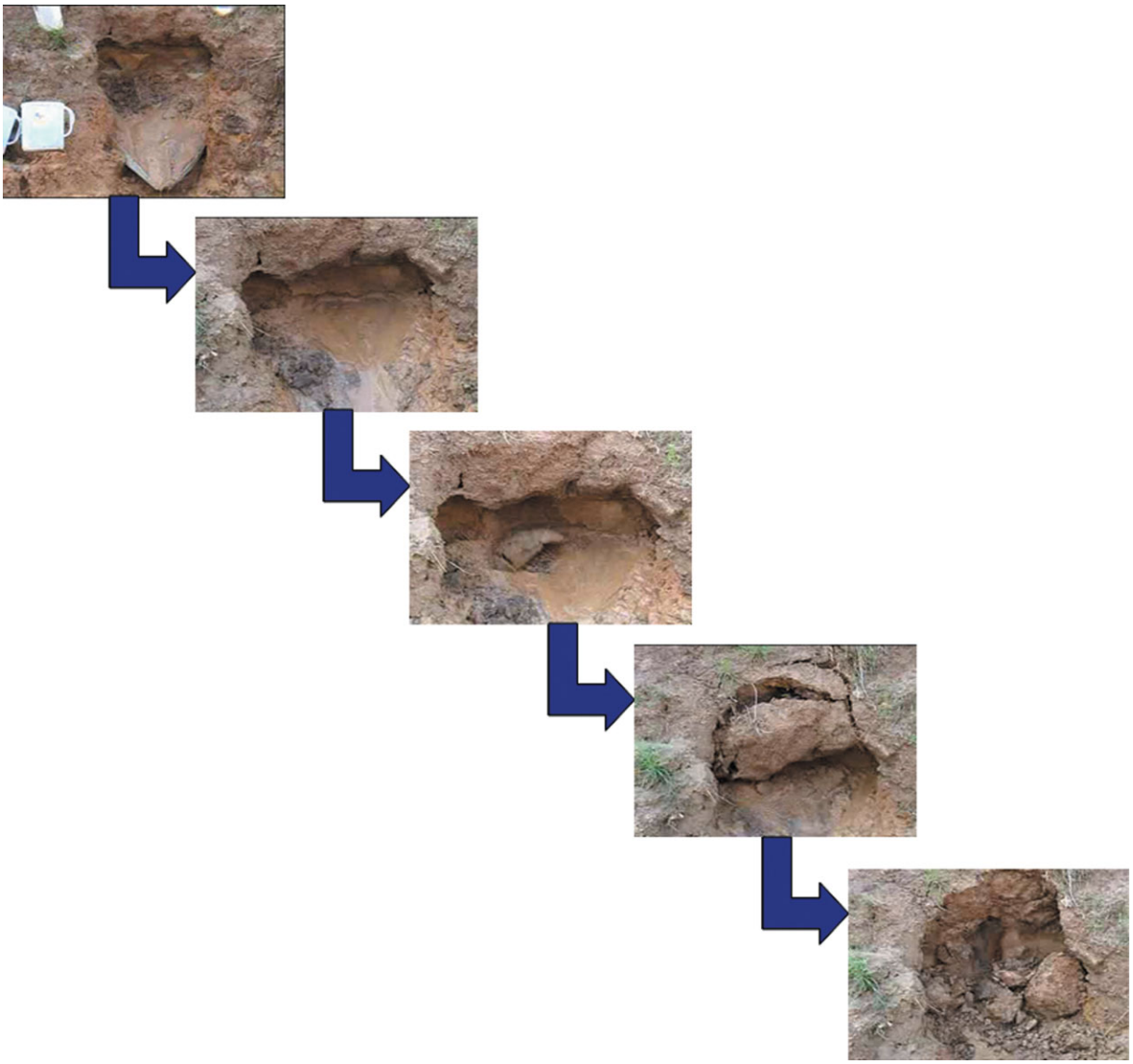

Figure 5. Time sequence of bank collapse by seepage flow at a buried seep at Goodwin Creek. The first picture shows the lateral flow collection pan used to measure seep discharge. Total elapsed time is approximately 30 minutes. This figure is available in colour online at www.interscience.wiley.com/journal/espl

buried seeps (Figures 4 and 5) and the following set of samples (three replicates) was obtained: vertical samples at 190 cm bgs (immediately above the conductive concretion layer), vertical samples at 210 cm bgs (Fe and Mn conductive concretion layer) and vertical samples at 230–260 cm bgs (loamy sand layer).

Samples were analyzed in the laboratory to determine particle size distribution, saturated hydraulic conductivity and the soil water retention curve. Particle size analysis was determined by the hydrometer method (Gee and Or, 2002). The saturated hydraulic conductivity was determined on undisturbed soil cores by the constant head method (Amoozegar and Wilson, 1999). Water retention was determined on undisturbed soil cores using Tempe cells for 0–1000 cm pressures. For pressures above 1000 cm, water retention was determined on disturbed soil samples by the pressure plate extractor method as described by Dane and Hopmans (2002). Water retention data were modeled with RETention Curve (RETC) with the van Genuchten equation using the Mualem assumption (van Genuchten *et al.*, 1991).

DOI: 10.1002/esp

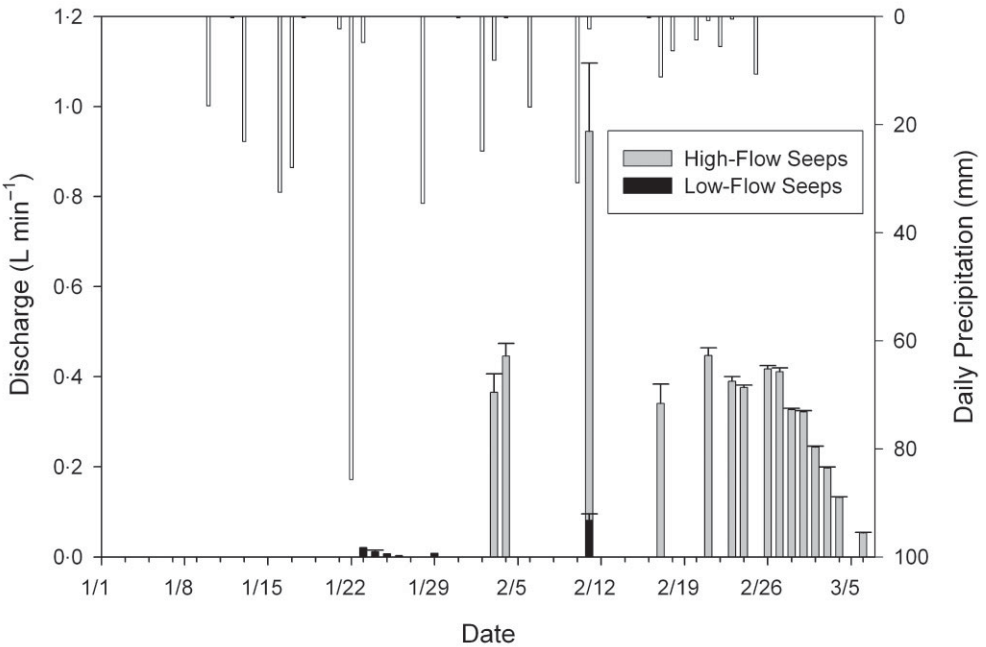

Figure 6. Correlation of daily precipitation (mm) and seepage discharge (L min^{-1}) at Goodwin Creek on specific sampling dates between 1 January and 7 March 2006.

Results and Discussion

Seepage Flow and Erosion

Seepage erosion measurements were made following significant (i.e. greater than 1·0 cm) rainfall events from 1 January 2006 through 1 May 2006, which correlated with the date that seepage terminated. Six seeps were measured throughout the study period and were grouped into three seep types: LF, HF and buried seeps. Three seeps fell within the LF category, with samples collected from four rainfall events. These seeps were the first seeps to become noticeably active during the study period in late January, following a precipitation event that caused stream stages to rise approximately 3 m above base flow levels (Figure 6). Seep flow rates were generally less than 0·05 L min^{-1} and increased to approximately 0·1 L min^{-1} during one event. Correspondingly, seep erosion rates were insignificant (i.e. less than 1 g min^{-1}). However, the importance of such seeps in long-term bank erosion cannot be overlooked. These seeps generally occurred directly above the cohesive early Holocene layers at Goodwin Creek that exhibited a blocky, prismatic structure with vertical fractures between the peds. Vertical fractures in the early Holocene layer occurred at a frequency of 2·3 per meter length of the bank face at the LF seep area. Subsequent rises in stream stage were then capable of causing these prismatic blocks to become unstable and collapse due to significant recharge of stream water into the bank and subsequent drainage following a fall in stream stage. It is also likely that the propensity of fractures in the layer below the laterally conductive concretion layer is the reason for the lower seepage rates in this area.

The second type of seep was classified as HF seeps that continued to flow throughout the study period once the streambanks had pore water pressures near saturation approximately 150–200 cm bgs. The HF seeps occurred at a specific 50 m reach along Goodwin Creek. The vertical fractures between peds in the loamy sand layer were only 1·3 per meter length of bank face. Two seeps fell within the HF classification with seep measurements after 10 rainfall events.

These HF seeps were similar to the seeps occurring as subsurface flow through a conductive loamy sand layer measured by Wilson *et al.* (2007) at Little Topashaw Creek. Wilson *et al.* (2007) observed seepage erosion on several occasions along an 800 m reach of the Little Topashaw Creek between February and July 2003. Most seeps occurred as subsurface flow through the loamy sand conductive layer above a less conductive clay loam soil layer. At Little Topashaw Creek, the seepage flow eroded sediment from the conductive, relatively noncohesive loamy sand layer, as simulated in the lysimeter experiments of Fox *et al.* (2006) and Wilson *et al.* (2007). The Goodwin Creek seeps originated

DOI: 10.1002/esp

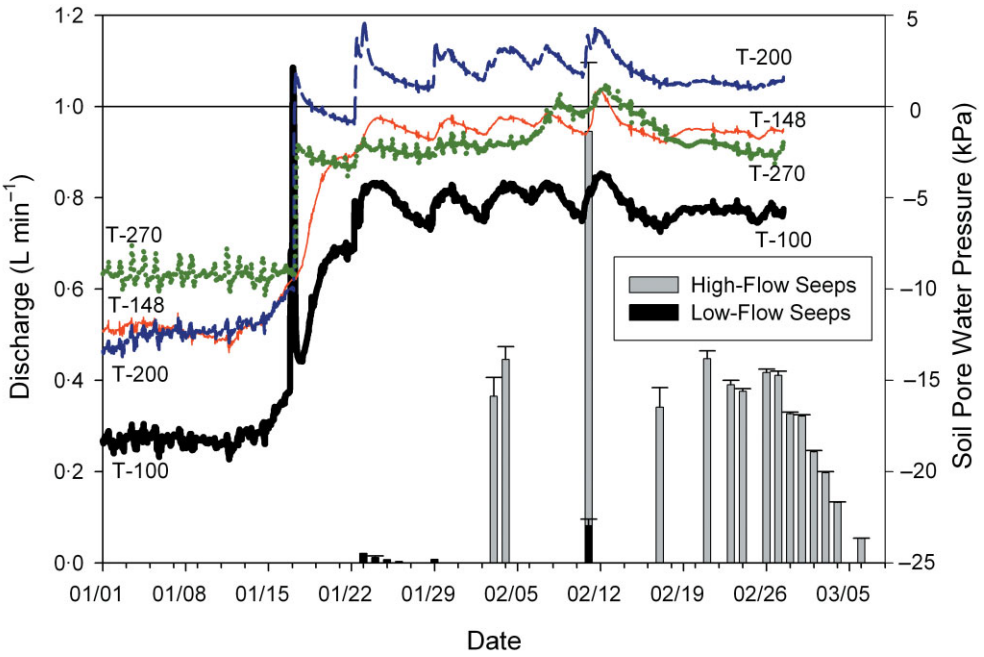

Figure 7. Correlation of tensiometer readings of streambank pore water pressure (kPa) and seepage discharge (L min^{-1}) at Goodwin Creek on specific sampling dates between 1 January and 7 March 2006. This figure is available in colour online at www.interscience.wiley.com/journal/espl

from the conductive concretion layer, but the flow eroded a less cohesive loamy sand layer below the conductive concretion layer. The saturation of the underlying sediment just below the Fe and Mn conductive concretion layer and at the face of the streambank along with the force of erosion due to seepage flow becoming overland flow initiated headcuts that continued to develop in size throughout the study period. These headcuts then resulted in mass failure of the concretion layer and the overlying silt loam topsoil, resulting in large sediment failure blocks (Figure 4).

Initiation of these HF seeps occurred on 3 February 2006 (Figure 7), as the tensiometer data suggested that soil pore water pressures approached near saturation (i.e. soil pore water pressures greater than −5 kPa), and terminated in the middle of April. Seep flow rates averaged 0·39 L min^{-1}, with a maximum of 1·02 L min^{-1} following a 6·0 cm rainfall event. These seepage flow rates were significantly greater ($\alpha = 0{\cdot}05$, P-value = 0·005) than the average seepage flow rates measured by Wilson *et al.* (2007) at Little Topashaw Creek, which averaged 0·15 m^3 d^{-1} and were fairly consistent between seeps, with a coefficient of variation (CV) of 62%.

Continuous sampling was performed following one event at Goodwin Creek in late February (25 February 2006) for seven days after the rainfall ceased. The decline in the seepage flow rate was slow during periods without rainstorm events (i.e. required seven days for seepage discharge to decline from just above 0·4 to 0·1 L min^{-1}), with the seepage discharge versus time represented by a sigmoidal function with $R^2 = 0{\cdot}99$ (Figure 8). These HF seep flow rates were slightly correlated to precipitation events and strongly correlated to measurements of streambank pore water pressure. A correlation matrix between the seep flow rates and the tensiometer readings suggests that the seep flow rates are most strongly correlated to the tensiometers at 270 cm bgs ($r = -0{\cdot}88$), followed by the tensiometer at 148 cm bgs ($r = -0{\cdot}76$) and then the tensiometer at 200 cm bgs ($r = -0{\cdot}61$).

Seepage erosion rates at Goodwin Creek averaged 16·0 g min^{-1} with a maximum of 68·0 g min^{-1}. Average and maximum sediment concentrations were 27·2 and 97·8 g L^{-1}, respectively (Figure 9). Even though the seepage flow rates at Goodwin Creek were greater than those at Little Topashaw Creek, the erosion rates and sediment concentrations at Goodwin Creek were on average significantly less ($\alpha = 0{\cdot}05$, P-value = 0·025) than those from loamy sand over restrictive layer seeps at Little Topashaw Creek, which exhibited liquefaction of the conductive layer with sediment concentrations averaging 250 g L^{-1} (CV of 93%). These results are reasonable considering the cohesiveness of the soil layers at each site.

The field measurements suggest that there exists a critical seep discharge or critical shear stress required to erode particles from the streambank face as seepage erosion became overland flow. In fact, the relationship between erosion

DOI: 10.1002/esp

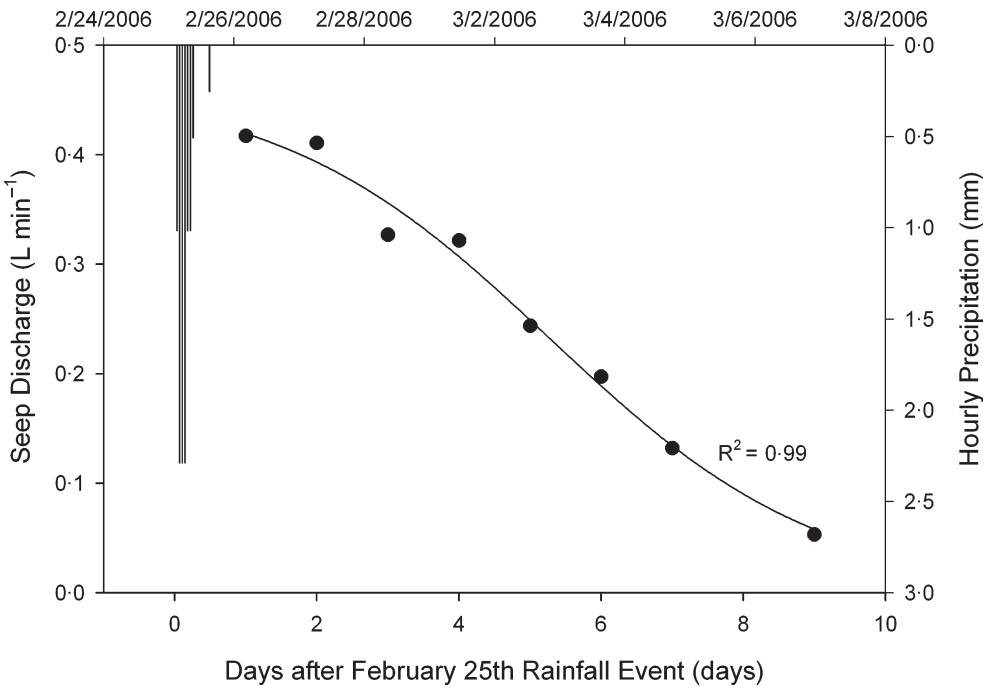

Figure 8. Seepage discharge (L min^{-1}) at a Goodwin Creek high-flow seep following the 25 February 2006 rainstorm event. Seep flow measurements were not made on day 8 after the 25 February event.

rate and discharge generally followed the excess shear stress equation (Figure 10). The equation fit to the seepage data uses seep flow rate in the place of shear stress due to our inability to measure shear stress in the field:

$$E_r = K_r(q - q_c)^a \tag{2}$$

where q_c is the critical seep discharge necessary to mobilize particles and K_r is a modified erodibility coefficient based on seep flow, not shear stress. Since seep flow rate corresponds to shear stress, it was observed that an excess shear stress equation fits the data well (R^2 = 0·61). The seepage erosion sediment transport model developed by Fox *et al.* (2006) was proposed to represent the intermittent mass wasting due to seepage flow, not the erosion of soil particles by seepage flow becoming overland flow. Therefore, for this situation, an equation based on excess shear stress is more appropriate.

However, the mathematical representation discussed above represents a simplification of the process. The erosion rate was dependent on not only the seep flow rate but also the history of the seep. For equivalent seep discharge, early events in the headcut formation resulted in greater sediment flux than events occurring later in the formation of the headcut (Figure 10). More sophisticated studies are needed to account for this 'time-history' of headcut formation by seepage flow.

The third type of seep was similar to the HF seeps except that these seeps were buried by sloughed bank material from previous bank failures (Figure 5). One seep location fell within the 'buried' seep classification and this seep was sampled following two rainfall events. Seep flows from buried seeps were intermittent as opposed to the more persistent HF seeps. These seeps only occurred during the peak flow events of HF seeps and generally consisted of considerable sediment volume due to the noncohesive nature of previous sloughed bank material. They also occurred at lower elevations on the streambank as compared to the HF seeps, most likely due to flow convergence within sloughed streambank material from several HF seeps. Their initiation was also delayed approximately 24–48 hr from the increase in seep flow rate at the HF seeps. They generally terminated within one or two days. Average measured flow rates for these seeps were 0·75 L min^{-1} with a maximum flow rate of 0·84 L min^{-1}, which was within the range of flow rates for the HF seeps immediately following rainfall events. Average erosion rates and sediment concentrations from these buried seeps were 738 g min^{-1} and 989 g L^{-1}, respectively, higher than even the peak erosion rates and sediment concentrations measured from the HF seeps, and of the order of seepage sediment concentrations measured by Wilson *et al.* (2007) at Little Topashaw Creek.

DOI: 10.1002/esp

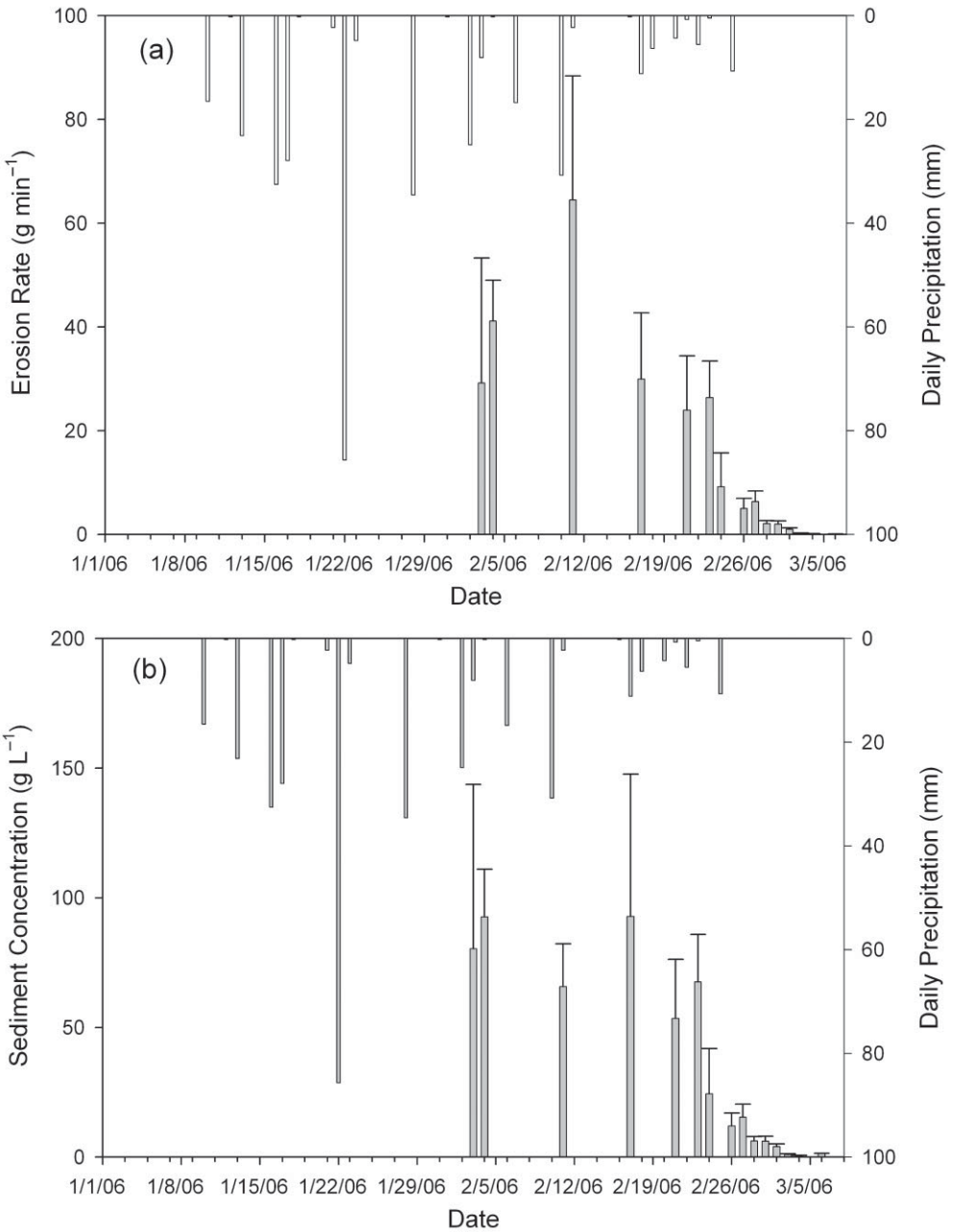

Figure 9. Seepage (a) erosion rate (g min^{-1}) and (b) sediment concentration (g L^{-1}) measurements at Goodwin Creek high-flow seeps on specific sampling dates between 1 January and 7 March 2006 and correlation to precipitation.

Streambank Characterization

Soil and macropore properties at both LF and HF seep locations are given in Table II. A key indication of the prevalence of the HF seeps was the elevation of the Fe and Mn concretion layer. The HF seeps were positioned where the concretion layer outcropped at a lower elevation, resulting in a ground water flow convergence zone. This lower elevation also resulted in the Fe and Mn conductive concretion layer being positioned just above the loamy sand layer at the streambank face. Formation of Fe and Mn concretions (i.e. redox-morphic features) was an indication of a fluctuating perched water table in which Fe and Mn precipitated out of solution as free water dissipated (D'Amore

DOI: 10.1002/esp

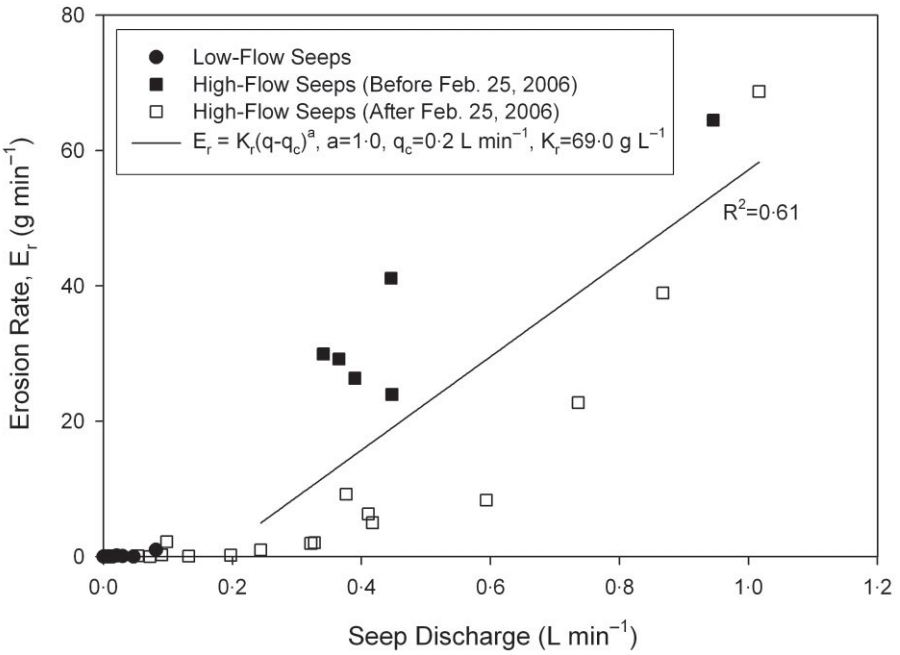

Figure 10. Correlation of erosion rate (g min^{-1}) and discharge (L min^{-1}) for high-flow and low-flow seeps at Goodwin Creek.

Table II. Soil and macropore properties at low flow (LF) and high flow (HF) seep locations. LH = late Holocene, EH = early Holocene, LS = loamy sand, CnL = Fe and Mn conductive concretion layer, V = vertically oriented sample and H = horizontally oriented sample

Seep	Layer	Depth (cm)		Texture	Sand %	Clay %	Bulk density, ρ g/cm^3 Mean (std dev.)	Saturated hydraulic conductivity, K_s cm/h Mean (std dev.)	Macropores #/m^2	
									>5 mm	1–5 mm
LF	LH	0–25	V	Silt Loam	15·0	12·3	1·41 (0·10)	5·73 (6·28)	40	688
LF	LH	25–150	V	Silt Loam	12·5	10·3	1·44 (0·06)	7·23 (2·12)	85	709
LF	LH	25–150	H				1·44 (0·05)	8·39 (8·52)		
LF	CnL	150–175	V	Loam	52·1	12·6	1·49 (0·11)	17·58 (13·65)	28	400
LF	CnL	150–175	H				1·47 (0·09)	29·36 (30·69)		
HF	CnL	200–215	V	Sandy loam	55·6	16·7	1·53 (0·17)	31·30 (47·62)		
LF	EH	>195	V	Silt loam	27·2	20·5	1·68 (0·09)	6·60 (5·52)		
HF	LS	>230	V	Loamy sand	85·5	5·8	1·69 (0·08)	3·34 (4·30)	11	277

et al., 2004; USACE, 1987). The lateral extent of the concentration layer into the bank and adjacent riparian zone is not known; however, its presence has been consistent throughout 11 years of monitoring with over 7 m of bank retreat.

Tensiometer data also suggested the presence of perched water table conditions. Correlation coefficients between tensiometer readings for T100, T148 and T200 were greater than 0·90, as opposed to correlation between T270 and

DOI: 10.1002/esp

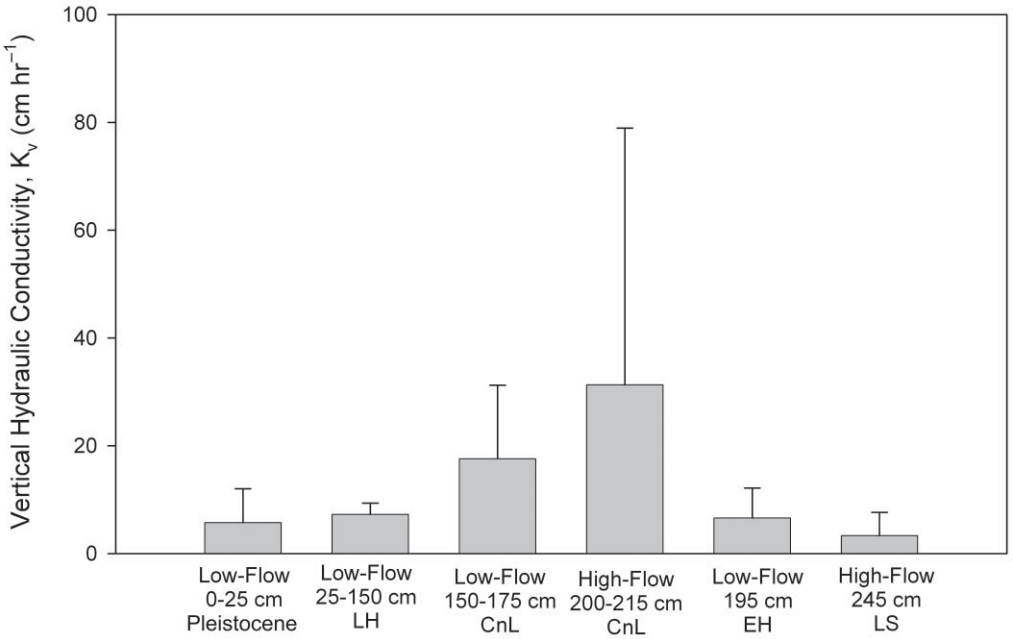

Figure 11. Illustration of vertical (K_v) hydraulic conductivity (cm hr^{-1}) measured from undisturbed soil samples taken from Goodwin Creek streambank. Depths correspond to distances below ground surface. LH = late Holocene, EH = early Holocene, CnL = concretion layer, LS = loamy sand.

T100, T148 and T200 of 0·43, 0·61 and 0·64, respectively. These results suggest the layers below the Fe and Mn conductive concretion layer do not respond to wetting front migration, and therefore water perched on top of this layer. Higher lateral K_s in the concretion layer (average of 29·4 cm hr^{-1} with a CV of 105%) allowed rapid interflow to the streambank face.

Hydraulic conductivity, K_s, contrast between the layers was less visible at Goodwin Creek (Figure 11) compared with Little Topashaw Creek, where Wilson *et al.* (2007) reported three orders of magnitude contrast in conductivity, but still important in controlling the flow patterns. There was a negligible difference in the vertical K_s between the late Holocene (5·7 and 7·2 cm hr^{-1}) and early Holocene (6·6 cm hr^{-1}) layers at the LF seeps, Table II. The vertical K_s of the early Holocene layer at the LF seep was about twice as high as the loamy sand layer (3·3 cm hr^{-1}) at the HF seep, which could explain a greater tendency to perch water.

The concretion layer between the late Holocene and either the early Holocene layer at the LF seep area or the loamy sand layer at the HF seep area appeared to be governing the hydrologic behavior of these streambank locations. At the LF seep, the vertical K_s of the concretion layer was almost three times higher than the vertical K_s of the underlying early Holocene. While the difference between vertical (7·2 cm hr^{-1}) and lateral K_s (8·4 cm hr^{-1}), Table II, in the upper late Holocene layer was negligible, the lateral K_s (29·4 cm hr^{-1}) was approximately double that of the vertical K_s (17·6 cm hr^{-1}) in the concretion layer. The anisotropy of the concretion layer resulted in the variability being much higher at both seep areas, with CV greater than 100%, than observed for the overlying late Holocene and underlying early Holocene or loamy sand layers. This anisotropy also contributed to the propensity of these sites to exhibit lateral flow, as evidenced by the fact that there was approximately three times greater lateral K_s in the concretion layer compared to the underlying vertical K_s.

Differences in water retention between the vertical and lateral samples were negligible as expected for all layers (Table III). Only minor differences were observed in the water retention curves for the two concretion layer sampling locations (Figure 12, Table III). However, the texture, cohesiveness and structure of the layer underlying the Fe and Mn conductive concretion layer were different at the LF and HF seep locations (Table II). The water retention curves suggested differences in water retention capacity between the underlying early Holocene and loamy sand layers (Figure 12, Table III). Water content at 10 000 cm was 0·14 cm^3 cm^{-3} and 0·03 cm^3 cm^{-3} for the early Holocene or loamy sand soil underlying the concretion layer at the LF and HF seeps, respectively. While the vertical K_s-values of these two soils were only slightly different (Figure 11), the unsaturated hydraulic conductivity, $K(h)$, estimated from the water retention curves, indicated that K(10 000 cm) was two orders of magnitude lower at the HF seep than at the

DOI: 10.1002/esp

Table III. RETention Curve (RETC) estimated water retention curve parameters (α, n) for soil samples at low flow (LF) and high flow (HF) seep locations. LH = late Holocene, EH = early Holocene, LS = loamy sand, CnL = Fe and Mn conductive concretion layer, V = vertically oriented sample and H = horizontally oriented sample

Seep	Layer	Depth (cm)		Saturated water content, θ_s ($cm^3\ cm^{-3}$)	Residual water content, θ_r ($cm^3\ cm^{-3}$)	α (cm^{-1})	n
LF	LH	25–150	V	0·50	0·02	0·003	1·55
LF	LH	25–150	H	0·50	0·02	0·002	1·64
LF	CnL	150–175	V	0·47	0·06	0·096	1·17
LF	CnL	150–175	H	0·44	0·05	0·075	1·18
HF	CnL	200–215	V	0·46	0·03	0·025	1·26
LF	EH	>195	V	0·40	0·05	0·008	1·23
HF	LS	>230	V	0·37	0·01	0·022	1·40

LF seep (Figure 2). Thus, the HF seep area dried out more quickly following flow events and wetted more slowly, thereby further enhancing the refraction of water laterally above this layer. The presence of the less cohesive loamy sand at the HF seep streambank face promoted headcut growth due to less shear stress required to mobilize soil particles.

One phenomenon of interest at Goodwin Creek that may contribute substantially to the potential for seepage flow is the occurrence of macropores in the late Holocene layer (Table II). Bank collapse commonly exposed large diameter macropores (i.e. up to 0·5 cm diameter) on the streambank face. Macropores were characterized by counting the number of macropores of two size classes within a prescribed area on the bank face (Table II). The number of macropores (i.e. greater than 1 mm diameter) in the late Holocene is approximately double the number of macropores in the concretion layer, which is about 50% higher than that in the underlying early Holocene. There is an even more dramatic difference in the number of large macropores (i.e. greater than 5 mm).

These macropores may allow rapid infiltration of water from the soil surface down to the concretion layer. While these macropores may be hydrologically active during storm events, they were generally inactive as soon as 6–12 hr following the rainfall event. This hypothesis was supported by two observations of seepage erosion at the site. First, some seeps increased their seepage flow rate as soon as 6–12 hr after termination of the rainfall event, suggesting rapid subsurface flow response to precipitation on the soil surface. Second, macropores in the late Holocene layer commonly exhibited sediment deposits on the bank face below the exposed pore from internal erosion (i.e. tunnel scour or pipe erosion).

Summary and Conclusions

This research reports on bank characterization and seepage flow measurements at a unique streambank site experiencing erosion by lateral, subsurface flow. Without detailed characterization of soil lithology, one would not have predicted the occurrence of seepage erosion due to the lack of vertical, conductivity contrast within primary bank layers. Bank characterization suggested less than an order of magnitude contrast in vertical, hydraulic conductivity between a conductive concretion layer and the underlying silt loam or loamy sand. Furthermore, small differences were observed in the water retention characteristics of the streambank layers. However, anisotropy contributed to the propensity of lateral flow, which was supported by tensiometer data that indicated the presence of perched water table conditions.

Unlike other ground water seeps reported in the literature, these seeps did not erode sediment from the conductive layer but rather sediment from layers that underlay the conductive layer. The headcuts formed due to the combined processes of reduced cohesion due to saturation of bank material and overland flow erosion from the discharging seep. Seepage flow and erosion measurements at Goodwin Creek suggested the presence of three different types of seep: intermittent LF seeps, primarily active following large rainstorm events and as a result of reverse bank storage, persistent HF seeps, which developed the most significant headcuts in the soil layer underneath the conductive layer, and buried seeps, which eroded unconsolidated bank material from previous bank failures. LF seeps acted in conjunction with overland flow and fluvial erosion to cause bank instability. The HF seeps resulted in the formation of headcuts, which caused bank collapse of both the conductive layer and the overlying silt loam topsoil. These HF seeps were persistent throughout the reporting period, initiating at near-saturation of bank material in early February and terminating during extended periods without rainfall in late April. Buried seeps originated from sloughed bank material from previous bank failures and resulted in the largest erosion rates and sediment concentrations.

DOI: 10.1002/esp

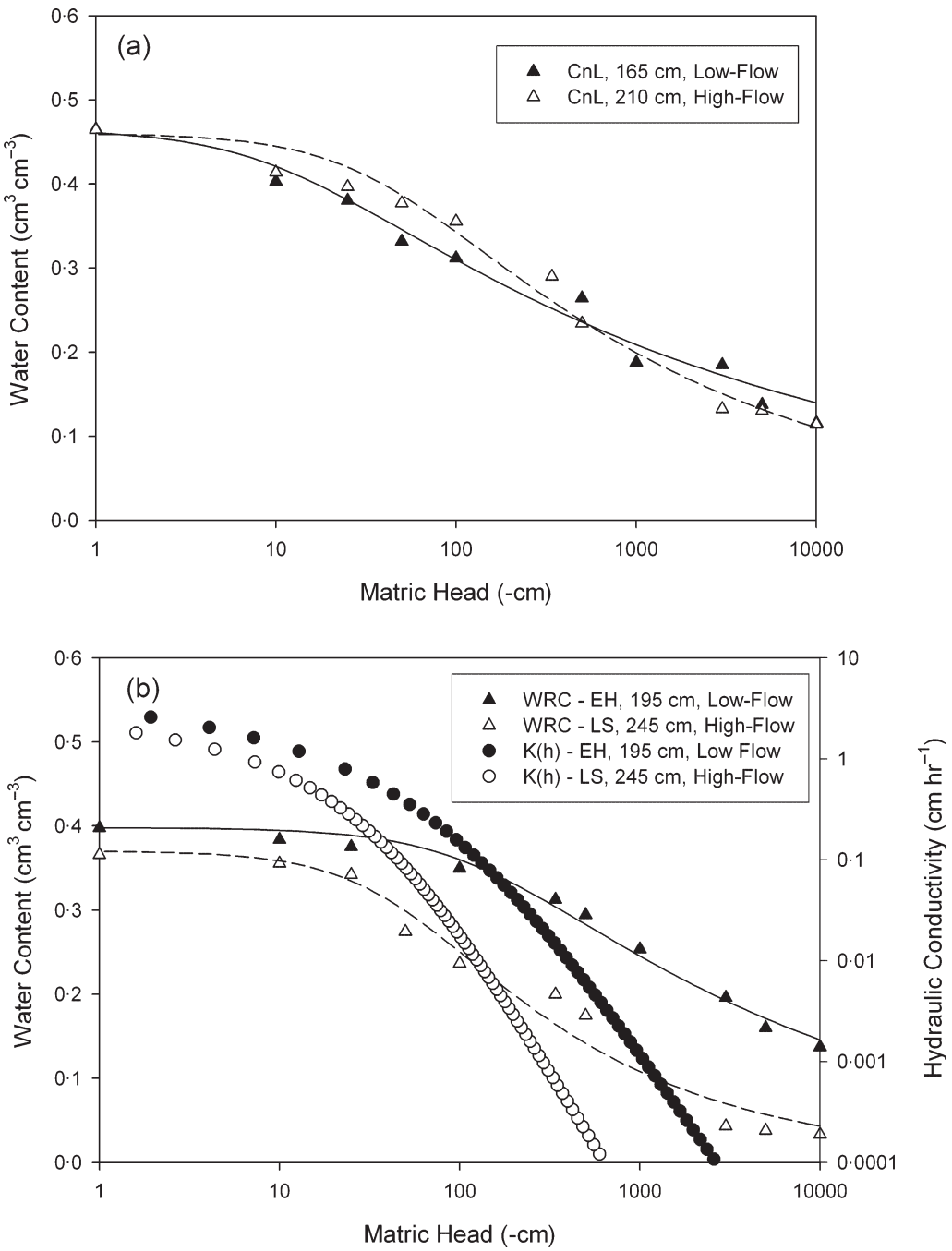

Figure 12. (a) Water retention curves (WRCs) for Fe and Mn conductive concretion layer (CnL) samples and (b) water retention curves (WRCs) and hydraulic conductivity, $K(h)$ (cm hr^{-1}), curves for early Holocene (EH) and loamy sand (LS) layers underlying CnL at low-flow and high-flow seep locations, respectively, along the Goodwin Creek streambank.

The interrelationship of seepage flow, overland flow and fluvial erosion makes it difficult to generalize the role of seepage erosion in bank instability. In cases where perched water table conditions exist and persistent HF seeps occur, the subsequent erosion and bank collapse of streambank sediment may be significant, especially in cases with buried seeps. The seepage erosion rates and sediment concentrations measured in this research does not take into account bank sloughing by undercutting. However, during the four-month study period, at least three bank collapses

DOI: 10.1002/esp

were observed as a result of the presence of seepage erosion undercutting the bank. The question that remains is whether seepage erosion, acting independently or combined with overland flow erosion, fluvial erosion and removal of negative pore-water pressures, is significant in the total sediment load to streams in these watersheds.

Acknowledgments

This material is based upon work supported by the Cooperative State Research, Education and Extension Service, US Department of Agriculture, under award No. 2005-35102-17209. The authors also acknowledge Brian Bell and Matthew Darr, USDA-ARS National Sedimentation Laboratory, and Amanda Fox for assistance in data collection and analysis. The authors acknowledge Dr. Massimo Rinaldi and an anonymous reviewer for comments that greatly improved the final manuscript.

References

Amoozegar A, Wilson GV. 1999. Methods for measuring hydraulic conductivity and drainable porosity. In *Agricultural Drainage*, Agronomy Monograph 38, Skaggs RW, Van Schilfgaarde J (eds). American Society of Agronomy: Madison, WI; 1149–1205.

Bingner RL. 1996. Runoff simulated from Goodwin Creek watershed using SWAT. *Transactions of the ASAE* **39**: 85–90.

Bryan RB, Hawke RM, Rockwell DL. 1998. The influence of subsurface moisture on rill system evolution. *Earth Surface Processes and Landforms* **23**(9): 773–789.

Bull LJ. 1997. Magnitude and variation in the contribution of bank erosion to the suspended sediment load of the River Severn, UK. *Earth Surface Processes and Landforms* **22**(12): 1109–1123.

Casagli N, Rinaldi M, Gargini A, Curini A. 1999. Pore water pressure and streambank stability: results from a monitoring site on the Sieve River, Italy. *Earth Surface Processes and Landforms* **24**(12): 1095–1114.

Coates DR. 1990. The relation of subsurface water to downslope movement and failure. In *Groundwater Geomorphology: the Role of Subsurface Water in Earth-Surface Processes and Landforms*, Geological Society of America Special Paper 252, Higgins CG, Coates DR (eds). Boulder, CO; 51–76.

D'Amore DV, Stewart SR, Huddleston JH. 2004. Saturation, reduction, and the formation of iron–manganese concretions in the Jackson-Frazier wetland, Oregon. *Soil Science Society of America Journal* **68**: 1012–1022.

Dane JH, Hopmans JW. 2002. Water retention and storage. In *Methods of Soil Analysis, Part 4 – Physical Methods*, Dane JH, Topp GC (eds). American Society of Agronomy: Madison, WI; 671–692.

Darby SE, Thorne CR. 1996. Numerical simulation of widening and bed deformation of straight sand-bed rivers. I. Model development. *Journal of Hydraulic Engineering* **122**: 184–193.

Dunne T. 1990. Hydrology, mechanics, and geomorphic implications of erosion by subsurface flow. In *Groundwater Geomorphology: the Role of Subsurface Water in Earth-Surface Processes and Landforms*, Geological Society of America Special Paper 252, Higgins CG, Coates DR (eds). Boulder, CO; 11–28.

Evans DJ, Gibson CE, Rossell RS. 2006. Sediment loads and sources in heavily modified Irish catchments: a move towards informed management strategies. *Geomorphology* **79**(1/2): 93–113.

Fox GA, Wilson GV, Periketi RK, Cullum RF. 2006. Sediment transport model for seepage erosion of streambank sediment. *Journal of Hydrologic Engineering* **11**(6): 603–611.

Gee GW, Or D. 2002. Particle-size analysis. In *Methods of Soil Analysis, Part 4 – Physical Methods*, Dane JH, Topp GC (eds). American Society of Agronomy: Madison, WI; 255–289.

Hagerty DJ. 1991a. Piping/sapping erosion. 1. Basic considerations. *Journal of Hydraulic Engineering* **117**(8): 991–1008.

Hagerty DJ. 1991b. Piping/sapping erosion. 2. Identification/diagnosis. *Journal of Hydraulic Engineering* **117**(8): 1009–1025.

Hanson GJ, Cook KR. 1997. *Development of Excess Shear Stress Parameters for Circular Jet Testing*, ASAE Paper 97-2227. American Society of Agricultural Engineers: St. Joseph, MI.

Hanson GJ, Simon A. 2001. Erodibility of cohesive streambeds in the loess area of the Midwestern USA. *Hydrologic Processes* **15**: 23–38.

Higgins CG. 1984. Piping and sapping: development of landforms by groundwater outflow. In *Groundwater and as a Geomorphic Agent*, Lafluer RG (ed.). Allen and Unwin: Boston, MA; 18–58.

Howard AD, McLane CF III. 1988. Erosion of cohesionless sediment by ground water seepage. *Water Resources Research* **24**(10): 1659–1674.

Istanbulluoglu E, Bras RL, Flores-Cervantes H, Tucker GE. 2005. Implications of bank failures and fluvial erosion for gulley development: field observations and modeling. *Journal of Geophysical Research – Earth Surface* **110**(F1). DOI: F01014

Iverson RM, Major JJ. 1986. Groundwater seepage vectors and the potential for hillslope failure and debris flow mobilization. *Water Resources Research* **22**(11): 1543–1548.

Jones JAA. 1997. Subsurface flow and subsurface erosion. In *Process and Form in Geomorphology*, Stoddart DR (ed.). Routledge: London; 74–120.

Langendoen EJ, Lowrance RR, Wiliiams RG, Pollen N, Simon A. 2005. Modeling the impact of riparian buffer systems on bank stability of an incised stream. In *Proceedings of the World Water and Environmental Resources Congress 2004*, Anchorage, AK, 2004, Walton R (ed.). DOI: 10.1061/40792

Langendoen EJ, Simon A, Pollen NL, Williams RG, Lowrance RR. 2006. A comprehensive stream-riparian corridor model to study the impact of riparian buffers on channel and edge-of-field processes: simulation of streambank hydrology. In *Proceedings of the Third Federal Interagency Hydrologic Modeling Conference*, Reno, NV, 2006 [CDROM].

Lobkovsky AE, Jensen B, Kudrolli A, Rothman DH. 2004. Threshold phenomena in erosion driven by subsurface flow. *Journal of Geophysical Research – Earth Surface* **109**(F4). DOI: F04010

Osman AM, Thorne CR. 1988. Riverbank stability analysis: I. Theory. *Journal of Hydraulic Engineering* **114**: 134–150.

Periketi RK. 2005. *Analysis of Seepage Erosion with Lysimeter Experiments and Numerical Modeling*, MS Thesis, Department of Civil Engineering, University of Mississippi, University, MS.

Rinaldi M, Casagli N. 1999. Stability of streambanks formed in partially saturated soils and effects of negative pore water pressures: the Siene River (Italy). *Geomorphology* **26**: 253–277.

Rinaldi M, Casagli N, Daporto S, Gargin A. 2004. Monitoring and modeling pore water pressure changes and riverbank stability during flow events. *Earth Surface Processes and Landforms* **29**: 237–254.

Sekely AC, Mulla DJ, Bauer DW. 2002. Streambank slumping and its contribution to the phosphorus and suspended sediment loads of the Blue Earth River, Minnesota. *Journal of Soil and Water Conservation* **57**(5): 243–250.

Simon A, Collison AJC. 2002. Quantifying the mechanical and hydrologic effects of riparian vegetation on streambank stability. *Earth Surface Processes and Landforms* **27**(5): 527–546.

Simon A, Curini A. 1998. Pore pressure and bank stability: the influence of matric suction. In *Water Resources Engineering '98*, Abt SR (ed.). American Society of Civil Engineers: New York; 358–363.

Simon A, Curini A, Darby SE, Langendoen EJ. 1999. Streambank mechanics and the role of bank and near-bank processes in incised channels. In *Incised River Channels*, Darby SE, Simon A (eds). Wiley: Chichester, UK; 193–217.

Simon A, Curini A, Darby SE, Langendoen EJ. 2000. Bank and near bank processes in an incised channel. *Geomorphology* **35**: 193–217.

Simon A, Darby SE. 1999. The nature and significance of incised river channels. In *Incised River Channels: Processes, Forms, Engineering and Management*, Darby SE, Simon A (eds). Wiley: New York; 3–18.

Thorne CR, Abt S. 1993. Analysis of riverbank stability due to toe scour and lateral erosion. *Earth Surface Processes and Landforms* **18**: 835–843.

US Army Corps of Engineers (USACE). 1987. *Corps of Engineers Wetlands Delineation Manual*, Technical Report Y-87-1. US Army Engineer Waterways Experimentation Station: Vicksburg, MS.

van Genuchten MTh, Leij FJ, Yates SR. 1991. *The RETC Code for Quantifying the Hydraulic Functions of Unsaturated Soils*, Version 1.0, EPA Report 600/2-91/065. US Salinity Laboratory, USDA, ARS: Riverside, CA.

Wilson GV, Jardine PM, Luxmore RJ, Zelazny LW, Lietzke DA, Todd DE. 1991. Hydrogeochemical processes controlling subsurface transport from an upper subcatchment of Walker Branch watershed during storm events: 1. Hydrologic transport processes. *Journal of Hydrology* **123**(3/4): 297–316.

Wilson GV, Periketi RK, Fox GA, Dabney SM, Shields FD, Cullum RF. 2007. Seepage erosion properties contributing to streambank failure. *Earth Surface Processes and Landforms* **32**(3): in press. DOI: 10.1002/esp.1405